Modelling of transition and noble metal vicinal surfaces: energetics, vibrations and stability

2003 J. Phys.: Condens. Matter 15 S3171

(http://iopscience.iop.org/0953-8984/15/47/001)

INSTITUTE OF PHYSICS PUBLISHING JOURNAL OF PHYSICS: CONDENSED MATTER

J. Phys.: Condens. Matter **15** (2003) S3171–S3196 PII: S0953-8984(03)67157-2

Modelling of transition and noble metal vicinal surfaces: energetics, vibrations and stability

C Barreteau[1], **F Raouafi**[1], **M C Desjonquères**[1] **and D Spanjaard**[2]

[1] DSM/DRECAM/SPCSI, CEA Saclay, F-91 191 Gif sur Yvette, France
[2] Laboratoire de Physique des Solides, Université Paris Sud, F-91 405 Orsay, France

Received 5 August 2003
Published 14 November 2003
Online at stacks.iop.org/JPhysCM/15/S3171

Abstract

The energetics of transition and noble metal (Rh, Pd, Cu) vicinal surfaces, i.e., the surface energy, step energy, kink energy and electronic interactions between steps, is studied at 0 K from electronic structure calculations in the tight binding approximation using an s, p and d valence orbital basis set. Then, the surface phonon spectra of copper are investigated in the harmonic approximation with the help of a semi-empirical inter-atomic potential. This allows one to derive the contribution of phonons at finite temperatures to the step free energy and to the interactions between steps. The last part is devoted to the stability of vicinal surfaces relative to faceting with special attention paid to the domain of orientations (100)–(111). Semi-empirical potentials are shown to be not realistic enough to give a reliable answer for this problem. The results derived from electronic structure calculations predict a variety of behaviours and, in particular, a possible faceting into two other vicinal orientations. Finally, temperature effects are discussed. Comparisons are made with other theoretical works and available experiments.

(Some figures in this article are in colour only in the electronic version)

1. Introduction

Studies of vicinal surfaces of metals have given rise to numerous experimental and theoretical works. Indeed the role of steps and kinks is fundamental for understanding the morphology of crystal surfaces and, in particular, its evolution with time and temperature as well as the equilibrium surface structure. In addition, vicinal surfaces may provide appropriate substrates for growing nanostructures, for instance nanowires, with magnetic and transport properties of high technological interest.

In the last 20 years the direct investigation of the local surface structure has become possible by the use of scanning probe microscopies such as scanning tunnelling microscopy (STM). Information on the energetics of surface defects can hence be derived from a statistical study of STM images and their evolution with temperature. For instance, the study of the

equilibrium shape of large adislands grown in homoepitaxy on monocrystalline surfaces has been used to determine the anisotropy of step energies and, more recently, the absolute values of step and kink energies [1]. Furthermore, the interaction between steps can be deduced from the study of terrace width distributions [2]. Kink energies can also be obtained from the observation of the spatial equilibrium fluctuations of step edges [3, 4]. In addition, experimental investigations of localized vibrational modes at vicinal surfaces have been carried out in the last decade by means of inelastic helium atom scattering (IHAS) [5] and electron energy loss spectroscopy (EELS) [6].

All these experimental results have motivated a lot of theoretical work. The study of the energetics of vicinal surfaces at 0 K starts from the determination of the surface energies as a function of the surface orientation. It has been investigated either by using semi-empirical potentials including an N body contribution such as in effective medium theory (EMT) [7, 8], the embedded atom method (EAM) [9], the second moment potential (SMA) [10–12] or starting from the determination of the electronic structure using the density functional theory (DFT) or the tight binding approximation (TB). However due to the very low symmetry of these systems, first principles calculations are scarce and limited to a very small number of geometries and metals: Al [13, 14], Cu [15, 16], Pt [17]. In contrast, in the case of transition metals, TB methods are able to describe correctly the quantum mechanical effects without a lot of computational effort. Using this method we have been able [18] to perform a systematic study of various vicinal surfaces of Rh, Pd and Cu as a function of the misorientation angle from which we have deduced step and kink energies as well as step–step interactions. The results of this work are reviewed in section 3, after a brief presentation of the geometry of vicinal surfaces (section 2).

Similarly *ab initio* methods have also been used to obtain localized vibration modes at vicinal surfaces but only the modes at high symmetry points of the Brillouin zone have been investigated [19, 20]. Central pair potentials in the harmonic approximation yield a reasonable description of vibration modes but not at a quantitative level. A good accuracy can be achieved with N body semi-empirical potentials such as that of the EAM [21, 22]. More recently we have set up a new potential for Cu [23] with which we have been able to reproduce accurately the phonon dispersion curves measured by means of IHAS [5] and EELS [6] on flat as well as on vicinal surfaces. In section 4 this potential is presented and the results concerning phonon dispersion curves and the vibrational contribution to the step free energy are summarized.

Finally, it is not obvious that all vicinal surfaces should be in thermodynamic equilibrium. Actually vicinal surfaces may decrease their surface free energy by rearranging the atoms in order to exhibit a hill and valley (or a factory roof) structure. This phenomenon, called faceting, is indeed observed in experiments and its occurrence can be predicted from the knowledge of the spatial anisotropy of the surface energy [24]. Using the results of sections 3 and 4. we have been able to re-examine [25, 26] this old problem in a realistic way. In section 5 we report our main results and discuss the implications of doing electronic structure calculations rather than using empirical potentials.

2. The geometry of vicinal surfaces

A vicinal surface is obtained by cutting a crystal along a plane making an angle θ with respect to a low index plane normal to the direction $\mathbf{n}_0$ (figure 1). For selected values of θ, such a surface can be viewed as a periodic succession of terraces normal to $\mathbf{n}_0$, with equal widths, separated by steps of monatomic height. The width of the terraces is determined by the number p of atomic rows (including the inner edge) parallel to the step edges. A vicinal surface corresponds to an atomic plane with high Miller indices. It can also be denoted using the Lang *et al* [27]

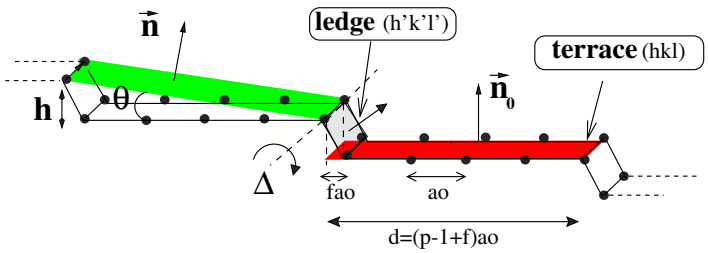

Figure 1. Step geometry of a $p(hkl) \times (h'k'l')$ vicinal surface.

Table 1. Geometrical features of the four types of vicinal surface. The geometry of the step edges is indicated by the distance between two consecutive atoms: nearest neighbours (nn), next nearest neighbours (nnn). The nature of the 2D unit cell is rectangular, either primitive (PR) or centred (CR). Finally the usual notation, step A and step B, for the vicinal surfaces of (111) is indicated.

Lang *et al* notation	Miller indices	f	Edge geometry	2D unit cell
$p(111) \times (100)$ step A	$(p+1,\ p-1,\ p-1)$	$2/3$	nn	p odd: PR p even: CR
$p(111) \times (\bar{1}11)$ step B	$(p-2,\ p,\ p)$	$1/3$	nn	p odd: CR p even: PR
$p(100) \times (111)$	$(1, 1, 2p-1)$	$1/2$	nn	CR
$p(100) \times (010)$	$(0,\ 1,\ p-1)$	0	nnn	p odd: CR p even: PR

notation $p(hkl) \times (h'k'l')$, (hkl) and $(h'k'l')$ being respectively the Miller indices of planes parallel to the terraces and to the ledges. Note also that when projecting the unit cell of the vicinal surface onto the terrace plane, a geometrical factor f occurs when the ledges and the terraces are not orthogonal.

In the following we consider FCC crystals and four step geometries with (111) and (100) terraces. The geometrical features of the four types of vicinal surface, denoted using Lang *et al* notation and Miller indices, are given in table 1. One can note that for a given step geometry there often exist two types of unit cell (primitive rectangular and centred rectangular) depending on the width of the terrace (p even or odd). In the first three geometries considered, the atoms along the step edges are first nearest neighbours while for the $p(100) \times (010)$ surface the atoms are second nearest neighbours and, consequently, the corresponding step edge has a zigzag shape that can be seen as a succession of kinks.

3. Electronic structure and energetics of vicinal surfaces in a tight binding model

3.1. The spd tight binding model

The study of the electronic structure of vicinal surfaces has been carried out using a slab model. The orientation of the normal to the vicinal surface is chosen first. A succession of N_{slab} atomic layers are built, N_{slab} being large enough that the interaction between the two free surfaces of the slab is negligible. The wider the terraces (i.e., the areas of the vicinal surface unit cell), the smaller the inter-layer spacing and the larger the number of layers N_{slab}. The system has thus a two dimensional (2D) periodicity with N_{slab} atoms per unit cell. *Ab initio* calculations are in principle feasible. However they are, at least up to now, limited to small terrace widths since they need a large amount of computer time. In contrast, the TB scheme is

very attractive since it is much less costly in computer time and still describes systems within the framework of quantum mechanics. Up to the last decade, the TB basis set was limited to the valence d (xy, yz, zx, $x^2 - y^2$, $3z^2 - r^2$) orbitals and this scheme was quite successful in explaining the general trends in the variation of a large number of physical properties along the transition series. However for FCC elements at the end of these series, the values of energetic quantities are then underestimated and even cancel for a full d band, due to the neglect of the contribution of the outer s and p (x, y, z) orbitals. Recently, it was found that it is possible to determine a transferable parametrized TB Hamiltonian in an spd basis set giving not only a quite good description of the band structure up to a few electronvolts above the d band, but also total energies with a good accuracy. This was initially proposed by Mehl and Papaconstantopoulos [28] who assumed a non-orthogonal basis set. Then it was shown [29] that for elements with a not completely filled d band, it was possible to reduce the number of parameters considerably by assuming an orthogonal basis set.

These models have been described in detail in [28, 29]; thus their main features are only briefly recalled in the following. The inter-atomic matrix elements of the Hamiltonian $H_{ij}^{\lambda\mu}$ (i, j: atomic sites; λ, μ: atomic orbitals) in the two centre approximation are determined from the ten Slater–Koster (SK) [30] hopping integrals ssσ, spσ, sdσ, ppσ, ppπ, pdσ, pdπ, ddσ, ddπ, ddδ. The laws of variation with distance of the SK hopping integrals are a simple exponential decay in [29] and are slightly more involved with a larger number of parameters in [28]. In the non-orthogonal scheme the overlap integrals $S_{ij}^{\lambda\mu}$ introduce also ten SK-like overlap parameters and their variations with distance follow the same kinds of law as the inter-atomic matrix elements of H. Following [28], in both schemes the intra-atomic matrix elements $H_{ii}^{\lambda\lambda}$, i.e., the atomic levels ε_{s}, ε_{p}, ε_{d}, are defined in such a way that the total energy is obtained by summing up the occupied energy levels. This means that all the other terms contained in the energy functional of the DFT have been taken into account by a rigid shift of the bulk band structure. As a consequence the atomic levels should depend on the atomic environment and are written in the form

$$\varepsilon_{i\lambda}^{0} = a_\lambda + b_\lambda \rho_i^{2/3} + c_\lambda \rho_i^{4/3} + d_\lambda \rho_i^2 \tag{1}$$

with

$$\rho_i = \sum_{j \neq i} \exp(-p_\rho (R_{ij}/R_0 - 1)) \tag{2}$$

where R_{ij} is the distance between atoms i and j and R_0 is a reference distance, usually the bulk equilibrium inter-atomic spacing.

The parameters of the model are determined by a non-linear least mean squares fit on the *ab initio* band structure and total energy for a few crystallographic bulk structures (usually FCC and BCC) at several inter-atomic distances. Their values for palladium and rhodium have been given in [29, 31] and for copper in [28, 32].

It should be noted that these parameters are obtained from systems in which all atoms are neutral since they are geometrically equivalent. When this is not the case we have added a shift δV_i to the on-site terms in order to ensure local charge neutrality which should be almost strictly obeyed in metals. Note that in the non-orthogonal case this induces also a modification $\delta V_{ij}^{\lambda\mu}$ of the inter-atomic elements of H [18]. These potentials arise from electron–electron interactions; thus one should subtract the corresponding double counting terms from the sum of occupied levels in the expression of the total energy which is then written in both schemes as

$$E_{\mathrm{tot}} = \sum_{n\ \mathrm{occ}} \epsilon_n - N_{\mathrm{val}} \sum_i \delta V_i \tag{3}$$

where N_{val} is the total number of valence spd electrons per atom of the metal.

3.2. The electronic structure

In order to apply the 2D Bloch theorem, a basis set of 2D Bloch waves localized in each layer l is defined as follows:

$$B_{l\lambda}(\mathbf{r}, \mathbf{k}_\parallel) = N_S^{-1/2} \sum_{i \in l} \exp(\mathrm{i}\mathbf{k}_\parallel \cdot \mathbf{R}_{i\parallel}) |i\lambda\rangle \tag{4}$$

where N_S is the number of atoms in each layer and $\mathbf{R}_{i\parallel}$ are the translation vectors of the 2D lattice. Using this basis set the solution of the Schrödinger equation can be written as

$$\Psi_{\mathbf{k}_\parallel, n}(\mathbf{r}) = \sum_{l\lambda} c^n_{l\lambda}(\mathbf{k}_\parallel) B_{l\lambda}(\mathbf{r}, \mathbf{k}_\parallel) \tag{5}$$

and the Hamiltonian and overlap matrices are reduced to $(9N_{\mathrm{slab}} \times 9N_{\mathrm{slab}})$ matrices $H^{\lambda\mu}_{ll'}(\mathbf{k}_\parallel)$ and $S^{\lambda\mu}_{ll'}(\mathbf{k}_\parallel)$. Then the equation

$$\sum_{l'\mu} [H^{\lambda\mu}_{ll'}(\mathbf{k}_\parallel) - \epsilon_n(\mathbf{k}_\parallel) S^{\lambda\mu}_{ll'}(\mathbf{k}_\parallel)] c^n_{l'\mu}(\mathbf{k}_\parallel) = 0 \tag{6}$$

is solved. Note that when the basis is orthonormal this equation reduces to a classical eigenvalue(vector) problem. In order to determine the projected band structure $\epsilon_n(\mathbf{k}_\parallel)$, $\mathbf{k}_\parallel$ is varied along symmetry lines of the surface Brillouin zone (SBZ). Other interesting quantities can be calculated such as the local density of states (LDOS) at layer l (per surface atom):

$$n_l(E) = \sum_{\substack{\lambda, n \\ l', \mu}} \frac{A}{(2\pi)^2} \int_{\mathrm{SBZ}} c^{n*}_{l\lambda}(\mathbf{k}_\parallel) S^{\lambda\mu}_{ll'}(\mathbf{k}_\parallel) c^n_{l'\mu}(\mathbf{k}_\parallel) \delta(E - \epsilon_n)\, \mathrm{d}^2\mathbf{k}_\parallel \tag{7}$$

where A is the area of the surface unit cell, or the spectral local DOS (per surface atom),

$$n_l(E, \mathbf{k}_\parallel) = \sum_{\substack{\lambda, n \\ l', \mu}} c^{n*}_{l\lambda}(\mathbf{k}_\parallel) S^{\lambda\mu}_{ll'}(\mathbf{k}_\parallel) c^n_{l'\mu}(\mathbf{k}_\parallel) \delta(E - \epsilon_n) \tag{8}$$

corresponding to a given value of $\mathbf{k}_\parallel$.

Some typical examples of surface projected densities of states, $n_l(E)$ and $n_l(E, \mathbf{k}_\parallel)$, have been given in [18] for several vicinal surfaces of rhodium. The most striking feature is the disappearance of almost all gaps. Indeed, as the width of the terraces increases, the area of the SBZ decreases and the height of the surface adapted bulk Brillouin zone (BBZ), i.e., the sampled domain of bulk states (corresponding to all possible values of k_z), increases accordingly and corresponds to lines with no symmetry in the BBZ. This explains the absence of gaps and of true surface states. However a number of resonances can be identified. When the terrace width tends to infinity the spectral DOS becomes vanishingly small in the energy domain corresponding to gaps in the projected band structure of the flat surface with the same orientation as the terraces.

3.3. Surface and step energies

The calculation of the total energy of the slab, from which surface and step energies are deduced, involves a summation over the SBZ which is carried out by using special $\mathbf{k}_\parallel$ points belonging to the irreducible part of the SBZ [33], each energy level being broadened by the derivative of a Fermi function of width w_F. The surface energy per surface atom of the vicinal surface is obtained from the following equation:

$$E_S(\mathbf{n}) = \frac{E_{\mathrm{slab}}(\mathbf{n}) - N_{\mathrm{slab}} E_{\mathrm{bulk}}}{2} \tag{9}$$

where $E_{\rm slab}$ is the total energy of the slab (with $N_{\rm slab}$ layers) per surface unit cell and $E_{\rm bulk}$ is the energy of a bulk atom. The corresponding surface energy per unit area is thus $\gamma(\mathbf{n}) = E_{\rm S}(\mathbf{n})/A(\mathbf{n})$ where $A(\mathbf{n})$ is the area of the surface unit cell.

The step energy per unit step length $\beta(\theta)$ of a vicinal surface is usually defined by the formula

$$\gamma(\mathbf{n}) = \gamma(\mathbf{n}_0)\cos(\theta) + \beta(\theta)\sin(\theta)/h \tag{10}$$

where h is the inter-planar distance along the direction $\mathbf{n}_0$ normal to the terraces. Note that due to the presence of the array of steps with a period depending on θ, $\beta(\theta)$ is expected to vary with θ as a result of step–step interactions. The value of the step energy for an isolated step is then obtained in the limit $\theta \to 0$. It is easy to show [34] that equation (10) can be transformed into a more convenient form:

$$E_{\rm step}(\mathbf{n}_0, p) = E_{\rm S}(\mathbf{n}_0, p) - (p - 1 + f)E_{\rm S}(\mathbf{n}_0, \infty) \tag{11}$$

where $E_{\rm step}(\mathbf{n}_0, p)$ is now the step energy per step atom of the vicinal surface in which the terraces of orientation $\mathbf{n}_0$ have p atomic rows parallel to the step edge (including the inner edge) and $E_{\rm S}(\mathbf{n}_0, p)$ ($E_{\rm S}(\mathbf{n}_0, \infty)$) is the surface energy per surface atom of the vicinal (flat) surface. Finally, f is a geometrical factor depending on the vicinal surface which has been defined in section 2 (figure 1).

The calculation of step energies and especially of their variation with p is rather tricky since the step energies are of the order of a few 10^{-1} eV and the magnitude of their variation with p is, at most, $\simeq 2 \times 10^{-2}$ eV. Thus the surface energies involved in (11) must be calculated with an accuracy of 10^{-3} eV. The parametrized TB Hamiltonian being given, the accuracy of the calculation is mainly governed by the thickness of the slab, the number of $\mathbf{k}_\parallel$ points in the irreducible part of the SBZ and the Fermi level broadening $w_{\rm F}$. Note that we have extrapolated the total energy at zero broadening using the usual approximation of [35]:

$$E_{\rm tot}(T = 0) \approx E_{\rm tot}(T) - \tfrac{1}{2} T S_{\rm e} + {\rm O}(T^2) \tag{12}$$

where $S_{\rm e}$ is the electronic entropy and T is the electronic temperature corresponding to the Fermi broadening $w_{\rm F}$. We have found that the required accuracy is achieved when using a number of vicinal planes in the slab $N_{\rm slab} = pn_{\rm slab}$ with $n_{\rm slab} \simeq 10$, 64 special $\mathbf{k}_\parallel$ points and a Fermi level broadening of 0.2 eV. Furthermore the iteration process ensuring the self-consistent charge neutrality condition was stopped when the difference in charge between two consecutive iterations was $<0.01{\rm e}^-$ per atom and the difference in total energy was smaller than 10^{-4} eV.

In table 2 the surface energies $\gamma(\mathbf{n})$ per unit surface area and $E_{\rm S}(\mathbf{n}_0, p)$ per surface atom are given as a function of p for the $p(100) \times (111)$ and $p(111) \times (100)$ surfaces. The step energies per step atom are deduced from (11) and are shown in figure 2 as a function of p. Typically terraces with $p \geqslant 6$ are wide enough for obtaining the asymptotic value, i.e., the isolated step energy with a numerical accuracy of $\simeq 10^{-3}$ eV. The values of the isolated step energies for Rh, Pd and Cu are given in table 3 for the four families of vicinal surfaces listed in table 1.

Let us compare our results with those deduced from the effective pair potential model proposed by Vitos *et al* [34]. In this model the energy of a bulk atom is written as

$$E_{\rm bulk} = -\sum_{R_J < R_{\rm c}} Z_{\rm b}^J V_J \tag{13}$$

where $Z_{\rm b}^J$ is the number of Jth neighbours at the distance R_J for a bulk atom and $R_{\rm c}$ the cut-off radius of interactions; the surface energy (per surface atom) is

$$E(\mathbf{n}_0, p) = \sum_{R_J < R_{\rm c}} n_{\rm S}^J V_J, \tag{14}$$

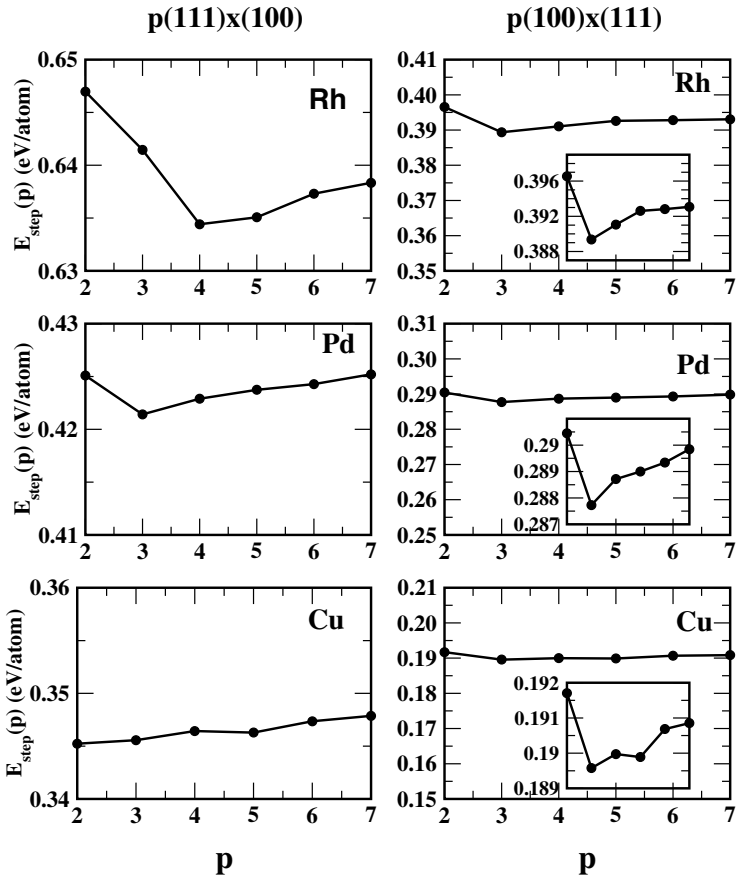

Figure 2. The variation of the step energy (per step atom) as a function of the terrace width for the $p(100) \times (111)$ (for which the energy scale has been enlarged in the insets to show clearly the sign of the interactions) and $p(111) \times (100)$ vicinal surfaces of Rh, Pd and Cu.

where n_S^J is the total number of Jth neighbours (per surface atom) suppressed by the surface. The step energies are then given by

$$E_{\text{step}}(\mathbf{n}_0, p) = \sum_{R_J < R_c} n^J_{\text{step}}(\mathbf{n}_0, p) V_J \tag{15}$$

with

$$n^J_{\text{step}}(\mathbf{n}_0, p) = n^J_S(\mathbf{n}_0, p) - (p - 1 + f) n^J_S(\mathbf{n}_0, \infty) \tag{16}$$

where $n^J_S(\mathbf{n}_0, p)$ and $n^J_S(\mathbf{n}_0, \infty)$ are, respectively, the total number of neighbours (per surface atom) in the Jth coordination shell suppressed by the vicinal and flat surfaces. In the work [34] of Vitos *et al* the effective pair potentials are limited to first, second and third neighbours (V_1, V_2, V_3) and their numerical values are derived from the (111), (100) and (110) surface energies. These surface energies are calculated using *ab initio* codes, the surface relaxation being neglected. Note that, due to the short range of the pair potentials, the numbers $n^J_{\text{step}}(\mathbf{n}_0, p)$ ($J \leqslant 3$) are constant as soon as p exceeds a given value p_∞ which is actually very small, i.e., most often $p_\infty = 2$. As a consequence this model ignores step–step interactions. Our calculations allow us to check the validity of this approach by using the pair potentials drawn from the surface energies obtained with the same parametrized TB Hamiltonian. The

Table 2. The surface energies γ (J m^{-2}) and E_S (eV/atom) of two families of vicinal surfaces. The surface area of the unit cell of a $p(100) \times (111)$ surface is $S = \sqrt{(2p-1)^2+2}a^2/4$ (a: lattice parameter) and the angle θ is given by $\tan\theta = \sqrt{2}/(2p-1)$. The corresponding quantities for the $p(111) \times (100)$ surface are $S = \sqrt{(p+1)^2+2(p-1)^2}a^2/4$ and $\tan\theta = 2\sqrt{2}/(3p-1)$.

	Rh ($a = 3.81$ Å)			
	$p(100) \times (111)$		$p(111) \times (100)$	
p	γ	E_S	γ	E_S
2	3.281	2.465	3.281	2.465
3	3.259	3.836	3.200	3.551
4	3.225	5.217	3.120	4.634
5	3.197	6.597	3.066	5.726
6	3.175	7.976	3.026	6.819
7	3.158	9.355	2.995	7.911
∞	3.044	1.379	2.781	1.091
	Pd ($a = 3.89$ Å)			
	$p(100) \times (111)$		$p(111) \times (100)$	
p	γ	E_S	γ	E_S
2	1.957	1.533	1.957	1.533
3	1.922	2.358	1.897	2.194
4	1.890	3.188	1.847	2.860
5	1.867	4.016	1.811	3.526
6	1.850	4.845	1.784	4.191
7	1.837	5.673	1.764	4.857
∞	1.754	0.828	1.625	0.665
	Cu ($a = 3.52$ Å)			
	$p(100) \times (111)$		$p(111) \times (100)$	
p	γ	E_S	γ	E_S
2	2.049	1.314	2.049	1.314
3	2.051	2.060	2.000	1.895
4	2.034	2.809	1.953	2.476
5	2.019	3.557	1.917	3.057
6	2.008	4.306	1.892	3.639
7	1.999	5.054	1.872	4.220
∞	1.935	0.748	1.734	0.581

expressions for the step energies are given in table 3 and their numerical values are very close to the values obtained from the previous method. Thus the method proposed by Vitos *et al* is quite valid for deriving a good estimate of the step energies when the low index surface energies and the step energy calculated from (11) are computed in the same manner. Indeed, we have compared our results with those obtained with the approach of Vitos *et al* [34, 36–38] by using other data sets for the surface energies. It is seen in table 3 that the agreement is reasonable save for Pd $p(100) \times (111)$ using the surface energy data set of Vitos *et al*. Actually, with the latter data V_2 is negative, while it is positive in the other calculations.

Finally note that in the effective pair potential model the step energy of vicinal surfaces with (111) terraces is the same for both ledge orientations (100), i.e., type A steps, and $(\bar{1}11)$,

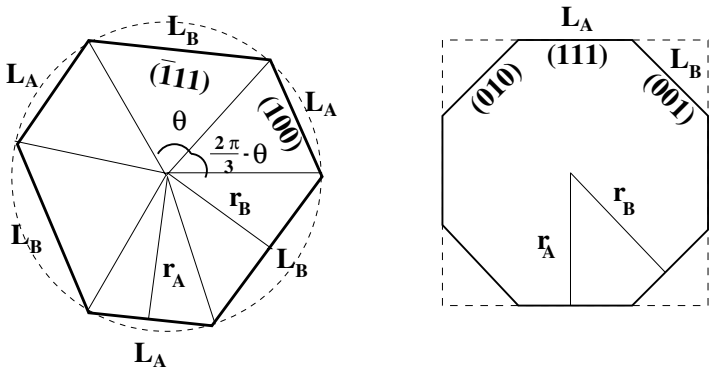

Figure 3. The equilibrium shapes of islands on (111) (a) and (100) (b) FCC surfaces. The orientations of the microfacets are indicated.

Table 3. Step energies for various vicinal geometries. Several types of result are presented: the full TB calculations and calculations based on effective pair potentials V_1, V_2, V_3 (EPP) fitted on the (111), (100) and (110) surface energies obtained from various methods: TB and *ab initio* methods [34, 36–38].

		Step energy E_{step} (eV/atom)						
			EPP					
	Vicinal surface $p \to \infty$	TB		TB	Vitos	Methfessel	Eichler	Galanakis
Rh	$p(111) \times (100)$	0.638	$2V_1 + 4V_3$	0.657	0.583	0.520	0.650	0.670
	$p(111) \times (\bar{1}11)$	0.645	$2V_1 + 4V_3$	0.657	0.583	0.520	0.650	0.670
	$p(100) \times (111)$	0.393	$V_1 + 2V_2$	0.407	0.288	0.265	0.295	0.285
	$p(100) \times (010)$	0.747	$2V_1 + 2V_2$	0.738	0.550	0.480	0.580	0.596
Pd	$p(111) \times (100)$	0.425	$2V_1 + 4V_3$	0.429	0.460	0.423		0.500
	$p(111) \times (\bar{1}11)$	0.432	$2V_1 + 4V_3$	0.429	0.460	0.423		0.500
	$p(100) \times (111)$	0.289	$V_1 + 2V_2$	0.295	0.106	0.222		0.298
	$p(100) \times (010)$	0.536	$2V_1 + 2V_2$	0.533	0.265	0.427		0.548
Cu	$p(111) \times (100)$	0.348	$2V_1 + 4V_3$	0.347	0.380			0.426
	$p(111) \times (\bar{1}11)$	0.345	$2V_1 + 4V_3$	0.347	0.380			0.426
	$p(100) \times (111)$	0.191	$V_1 + 2V_2$	0.192	0.200			0.241
	$p(100) \times (010)$	0.352	$2V_1 + 2V_2$	0.359	0.363			0.456

i.e., type B steps (see table 3), while in the full TB calculation step A is slightly energetically favoured for Rh and Pd, the reverse being found for Cu. This has some consequences for the equilibrium shape of large adislands in homoepitaxy as will be shown below.

Let us now compare our results with experimental data. The ratio of step energies and their absolute values can be directly determined, by means of STM, from the observation, as a function of temperature, of the equilibrium shape of the 2D adislands in homoepitaxy on a surface. On the (111) surface the adislands should show threefold symmetry. Consequently their shape is hexagon-like with alternating A- and B-type edge segments (see figure 3). When the two step energies are equal, the A and B segments have equal lengths and the hexagon is regular. Otherwise the ratio L_A/L_B of the lengths of A and B segments can be derived from β_A/β_B by applying the Wulff theorem. Experimental results are only available for Cu. The most recent experiments of Giesen [1] give an average step energy for the two kinds of step

on Cu(111) equal to 0.27 ± 0.03 eV per step atom, the energy of step A being measurably $(1.1 \pm 0.7\%)$ larger than that of a B step. Other published results [39, 40] on the average step energy lie between 0.22 and 0.31 eV. Our full TB calculations (see table 3) are in very good agreement with experiments for the ratio β_A/β_B. However they seem to slightly overestimate the average step energy. On the (100) surface the adislands should show a fourfold symmetry. Accordingly, the simplest polygonal shapes are a perfect square with (111)-type ledges and a square with broken corners with both (111)- and (010)-type ledges (respectively A and B; see figure 3). It can be easily shown [18] that when $E^A_{step}/E^B_{step} \leqslant 1/2$ the equilibrium shape is a perfect square and it is a square with broken corners otherwise. The experimental results of Giesen [1] show unambiguously square adislands with broken corners from which Giesen deduce the ratio $E^A_{step}/E^B_{step} \simeq 0.57$ to be compared to our full TB calculations that give 0.54. The calculated energy of the step (100) $\times$ (111) is 0.191 eV, also in good agreement with the experimental results $(0.22 \pm 0.02$ eV).

3.4. Step–step electronic interactions

Let us now discuss step–step interactions. There exist several types of interaction between steps. The most studied is the so-called elastic interaction due to the deformation fields around each step which interact repulsively. This elastic interaction gives rise in the continuum elasticity limit to an energy term varying at large inter-step distance as $1/d^2$ where d is the distance between two consecutive steps [41]. However as we will see below (section 4.2), when trying to fit results derived from empirical potentials on relaxed surfaces, it appears that for smaller d ($d \leqslant 6$ inter-row spacings) the behaviour of $E_{step}(d)$ deviates significantly from this law [42–45]. Furthermore meandering steps cannot cross each other. This gives rise to an entropic repulsive interaction varying as $1/d^2$ at large d [46]. Charge transfers in the vicinity of the steps produce a dipole–dipole interaction (repulsive or attractive) varying also as $1/d^2$.

Finally oscillatory electronic interactions of the Friedel type (i.e., arising from the interference between electron density oscillations around steps which have been visualized by STM [47]) should also be present similarly to those existing between chemisorbed atoms or defects [48, 49] but they have attracted little attention, at least up to now. Such interactions have been invoked by Frohn *et al* [50] to explain their STM observations on Cu(11 n). They have been introduced theoretically for cubium with a TB s band by Redfield and Zangwill [51] and discussed in a phenomenological manner by Pai *et al* [2]. A calculation of these interactions for vicinal surfaces of W(110) has also been carried out using a modified fourth moment approximation to TB theory for a pure d band [52]. However until recently there were no detailed electronic structure calculations on this subject, except one preliminary attempt with a TB scheme for FCC transition metals with a pure d band showing that these oscillatory interactions do exist [53]. General trends were put forward but the results were not quantitative due to the role played by sp electrons in the total energy, which is significant in FCC transition metals. The spd TB model described above avoids this approximation. Three main features can be extracted from figure 2:

(i) the step–step electronic interaction has a damped behaviour which is most often oscillatory,
(ii) the amplitude of the oscillations can be as large as some 10^{-2} eV for small values of p and remains of the order of some 10^{-3} eV when $p \geqslant 5$ in the domain of p studied,
(iii) the shape of the oscillations is quite stable for two neighbouring elements in the periodic table (rhodium and palladium) but it is dependent on the orientation of the steps.

Let us now compare our results with related works. The electronic step–step interaction energies are of the same order of magnitude as the full step–step interactions derived from

Table 4. Kink energies for various steps with close-packed edges in Rh, Pd and Cu (in eV).

(Terrace) × (ledge)	Rh	Pd	Cu		
			This work	Other calculations	Experiments
(111) × (100)	0.339	0.249	0.143	0.092 [15]	0.113 ± 0.007 [1]
(111) × ($\bar{1}$11)	0.329	0.242	0.148	0.117 [15]	0.121 ± 0.007 [1]
(100) × (111)	0.349	0.247	0.146	0.139 [54]	0.123 [4], 0.129 ± 0.009 [1]
V_1	0.332	0.238	0.166		

experiments by using an analysis of terrace width distributions which most often assumes purely repulsive interactions varying as $1/d^2$. This suggests that, as already mentioned [2], such interactions should be included in the treatment of experimental data. Nevertheless, it remains difficult to fit our results by an analytical expression and extrapolate an asymptotic behaviour to compare with elastic interactions.

Unfortunately they are only a few experimental data in the domain of small terrace widths. However an anomalous behaviour of the terrace width distribution at low temperatures for Cu $p(100) \times (111)$ has been observed by Frohn *et al* [50] which could be interpreted as due to a repulsive interaction when $d \simeq 1$–2 (in units of the nearest neighbour distance) but attractive (or oscillatory) when $d \simeq 3$–5. This is quite consistent with our results (figure 2).

Finally kink formation energies have been calculated within the same TB method [18] and the geometry suggested by Feibelman [15]. The results are given in table 4 and compare favourably with existing experiments and other calculations [15, 54].

4. Vibrational properties of Cu vicinal surfaces

The presence of steps on a surface modifies the electronic structure (see section 3) as well as the vibrational states, compared to the flat surface with the same orientation as the terraces. In the following we will use an empirical potential to investigate the vibrational states of vicinal surfaces of copper and deduce the contribution of phonons to the free energy of steps.

4.1. The empirical potential

The empirical potential used to describe the inter-atomic interactions of a set of atoms located at $\mathbf{R}_i$ is of the form

$$V(\mathbf{R}_1, \ldots, \mathbf{R}_i, \ldots) = A \sum_{i,j,j\neq i} (R_0/R_{ij})^{p_r} f_c(R_{ij}) - \xi \sum_i \left[\sum_{j\neq i} \exp[-2q(R_{ij}/R_0 - 1)] f_c(R_{ij}) \right]^{\alpha} \quad (17)$$

where R_{ij} is the distance between atoms i and j, R_0 is a reference distance that we take equal to the bulk nearest neighbour spacing, $f_c(R) = 1/(1 + \exp[(R - R_c)/\Delta])$ is a smooth cut-off function with a cut-off radius R_c, α is an exponent set equal to 2/3, and $\Delta = 0.05$ Å.

The parameters A, ξ, p_r and q are fitted to the experimental values of the cohesive energy E_c ($E_c = -3.5$ eV/atom) and of the three elastic constants, i.e., the bulk modulus ($B = 10.470$ eV/atom) and the two shear moduli C and C' ($C = 6.046$ eV/atom, $C' = 1.917$ eV/atom). The equilibrium equation at $R_0 = 2.5526$ Å gives a relation between the four parameters.

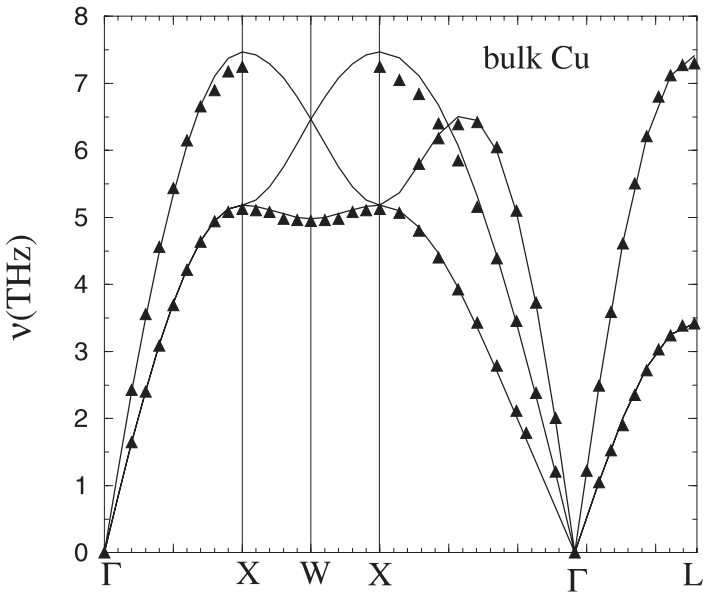

Figure 4. Phonon dispersion curves of bulk copper. The full lines correspond to the calculated dispersion curves and the triangles to the phonon frequencies measured from neutron inelastic scattering experiments [55]. Each segment along the path $\Gamma(\Delta)X(Z)W(Z)X(\Sigma)\Gamma(\Lambda)L$ is proportional to its length in reciprocal space.

We have determined by a least mean squares fit the sets of parameters obtained with different radii R_c for which interactions are cut off beyond first, second, third and fourth neighbours. For each set of parameters we have compared the fitted values of E_c, B, C, C', the surface relaxation of low index surfaces and the bulk phonon spectra to experiments. Let us note that we have also tried other sets of exponents for α but the choice of $\alpha = 2/3$ greatly improved the surface energies compared to *ab initio* data [23].

The best set of parameters is obtained for a cut-off radius $R_c = 4.02$ Å between second and third neighbours and the corresponding parameters are $A = 0.206$ eV, $\xi = 1.102$ eV, $p_r = 7.206$, $q = 2.220$. Indeed with this potential (hereafter referred to as P_2) the fit of E_c, B, C and C' is excellent (better than 1 meV per atom). When the potential includes only first nearest neighbours the shear moduli are not well reproduced and, in particular, C is about 25% smaller than the experimental value. The inclusion of third and fourth neighbours has a smaller influence on the elastic constants but the general tendency is an underestimation of the inward surface relaxation as one increases the cut-off radius beyond the second neighbours. We must emphasize that surface relaxation is important to get the local modifications of force constants correctly.

To obtain the phonon dispersion curves in the harmonic approximation the dynamical matrix is calculated from the analytical expression for the potential (17) and diagonalized for wavevectors **k** following symmetry lines in the BBZ. The calculated bulk dispersion curves are presented in figure 4. The agreement with experiment [55] is excellent. Apart from at the top of the spectrum at points X and L where the deviation between calculated and experimental frequencies is around 0.2 THz, the deviation is less than 0.1 THz. Note also that the shallow minimum at W in the lowest frequency band along XWX is reproduced only when R_c is chosen between second and third nearest neighbours.

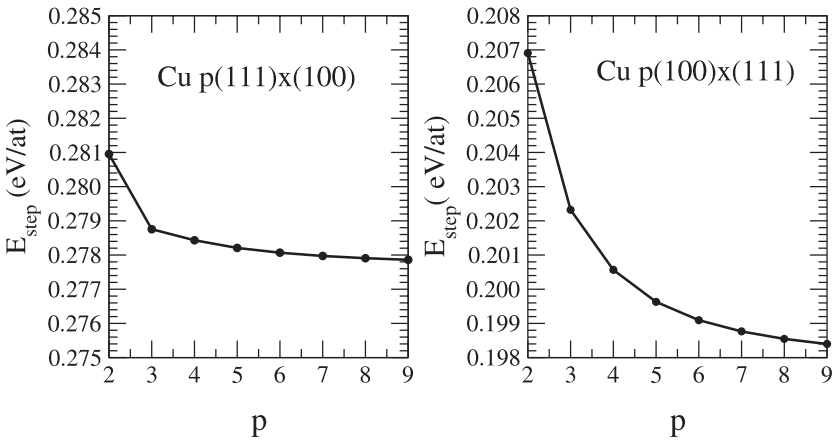

Figure 5. The variation of the step energy per step atom, for the $p(100) \times (111)$ and $p(111) \times (100)$ vicinal surfaces, as a function of the terrace width p. The geometry has been fully relaxed.

We have also calculated the surface projected band structure of the phonons for the three low index surfaces (111), (100) and (110) using the usual slab geometry. Our results were compared with available experimental EELS and IHAS data. The agreement is excellent for the three surfaces [23]. Low frequency as well as high frequency surface localized modes are reproduced with a surprising accuracy which is a good check of the transferability of the potential since surface modes are extremely sensitive to local modifications of the force constants due to the surface relaxation.

4.2. Atomic relaxation and elastic step–step interactions

The first task is the determination of the equilibrium atomic structure which is obtained by a standard conjugate gradient method. A common feature for most metallic vicinal surfaces is that all atoms, save at the inner edge, relax inwards, i.e., towards the bulk similarly to low index surfaces. However the direction of relaxation changes with the position of the atomic row on the terrace and one can identify a vortex-like structure described in a recent paper by Prévot *et al* [56]. The outer edge step atom (SC: step chain) always shows the largest inward relaxation; therefore the distance between the outer edge atom and its first nearest neighbour having the bulk coordination (BNN) exhibits the largest contraction compared to the bulk equilibrium nearest neighbour distance. As will be seen later the shortening of SC–BNN bonds produces a stiffening of the associated force constant. The inner edge atoms, unlike the other terrace atoms, relax outwards. Another feature common to all metallic vicinal surfaces is the profile of the multilayer relaxation, defined as the ratio of the distance between two adjacent atomic planes parallel to the vicinal surface with respect to the corresponding bulk inter-layer spacing. The multilayer relaxation always shows a damped oscillatory behaviour with a period of oscillation equal to the vicinality p of the surface [23, 42].

The equilibrium structure of a vicinal surface with a given terrace width p being known, it is straightforward to calculate the corresponding step energy per atom $E_{\mathrm{step}}(\mathbf{n}_0, p)$ using equation (11). $E_{\mathrm{step}}(\mathbf{n}_0, p)$ varies with the terrace width p as a result of step–step interactions. The step energy is obtained in the limit $p \to \infty$. In figure 5 we have presented the step energy per step atom for the vicinal $p(100) \times (111)$ and $p(111) \times (100)$ surfaces for p ranging from 2 to 9. $E_{\mathrm{step}}(\mathbf{n}_0, p)$ strictly decreases when p increases as expected from a calculation based on

a semi-empirical potential, since no oscillatory electronic effects are taken into account [18]. This variation is the result of purely elastic step–step interactions which are known to be repulsive from elasticity theory and, as mentioned previously, this term should vary at large inter-step distances as $1/d^2$ where d is the distance between two adjacent steps [41]. In order to compare the present results with the prediction of the elasticity theory we have fitted the step energy per step atom E_{step} as a function of $d = (p - 1 + f)a_0$ where a_0 is the distance between two adjacent atomic rows on the terrace plane ($6 \leqslant p \leqslant 100$), with an expression of the form $A_0 + A_2/d^2 + A_3/d^3$. In the case of Cu $p(100) \times (111)$ surfaces, $f = 0.5$ and $a_0 = R_0$. The results are $A_0 = 0.198$ eV, $A_2 = 0.322$ eV Å^2 and $A_3 = -0.955$ eV Å^3. A_0 is the asymptotic value giving the step energy of an isolated step and is in very good agreement with the value given by TB calculations (see table 3). It is interesting to note that the coefficients A_2 and A_3 have opposite signs similarly to what was found on $p(100) \times (010)$ surfaces of Ni and Au in a previous atomistic study [57]. Although A_3 is non-zero, its contribution becomes negligible for p larger than 10.

4.3. Projected phonon band structure of vicinal surfaces

The vibrational spectra of various vicinal surfaces have been presented in a recent paper [23]. Thus, the most important features will be illustrated here for two specific cases for which detailed experimental IHAS [5] and EELS [6] data are available for phonons propagating parallel and perpendicular to the step edge on the (211) and (511) surfaces.

There are several common features of the surface projected band structure of vicinal surfaces. First the most striking feature is the disappearance of almost all gaps in any direction of $\mathbf{k}_\parallel$ space, for the same reason as already explained in the electronic structure section. Second, the localized modes propagating perpendicular to the terraces have a clear back-folded structure. This back-folding leads to optical modes, their number increasing with the terrace width. Third, the localized modes propagating parallel to the step edge show a strong similarity with the corresponding modes of the low index surface with the same terrace orientation. Finally some resonant or localized modes in the vicinity of the steps also appear. In particular, a very specific mode is present in almost all dispersion curves at the very top of the band edge. This state is purely localized on the BNN atoms and is closely related to the stiffening of the force constant mentioned above.

These general features are seen in the surface projected phonon band structure of the (211) and (511) surfaces, i.e., with the Lang *et al* notation $3(111) \times (100)$ and $3(100) \times (111)$. Indeed, in figure 6, the only noticeable small gap is around the $\bar{\text{X}}$ point for the (211) surface, whereas all gaps have disappeared for the (511) surface. Let us consider the $\bar{\Gamma}\bar{\text{X}}$ and $\bar{\Gamma}\bar{\text{Y}}$ directions corresponding to directions of propagation parallel and perpendicular to the step edges, respectively. Along the $\bar{\Gamma}\bar{\text{X}}$ direction of the (211) surface, the most prominent surface features are a transverse mode (T), horizontally polarized, the sagittal Rayleigh mode (R) and a step localized mode (E). In addition another localized mode is found around the middle of the gap at $\bar{\text{X}}$. The same types of mode are also found on the (511) surface. Moreover there is a weakly localized longitudinal mode (L) which, actually, is also present on the (211) surface but is even less localized. All these results are in very good agreement with IHAS and EELS data. Modes propagating perpendicularly to the step (along $\bar{\Gamma}\bar{\text{Y}}$) can be qualitatively described as resulting from 'back-folding' [58] of the Rayleigh and transverse modes. Note that the mode localized on the BNN atom is particularly visible on the (511) surface for which the z component of the force constant between the BNN and step edge atom is 44% larger than the bulk one [23].

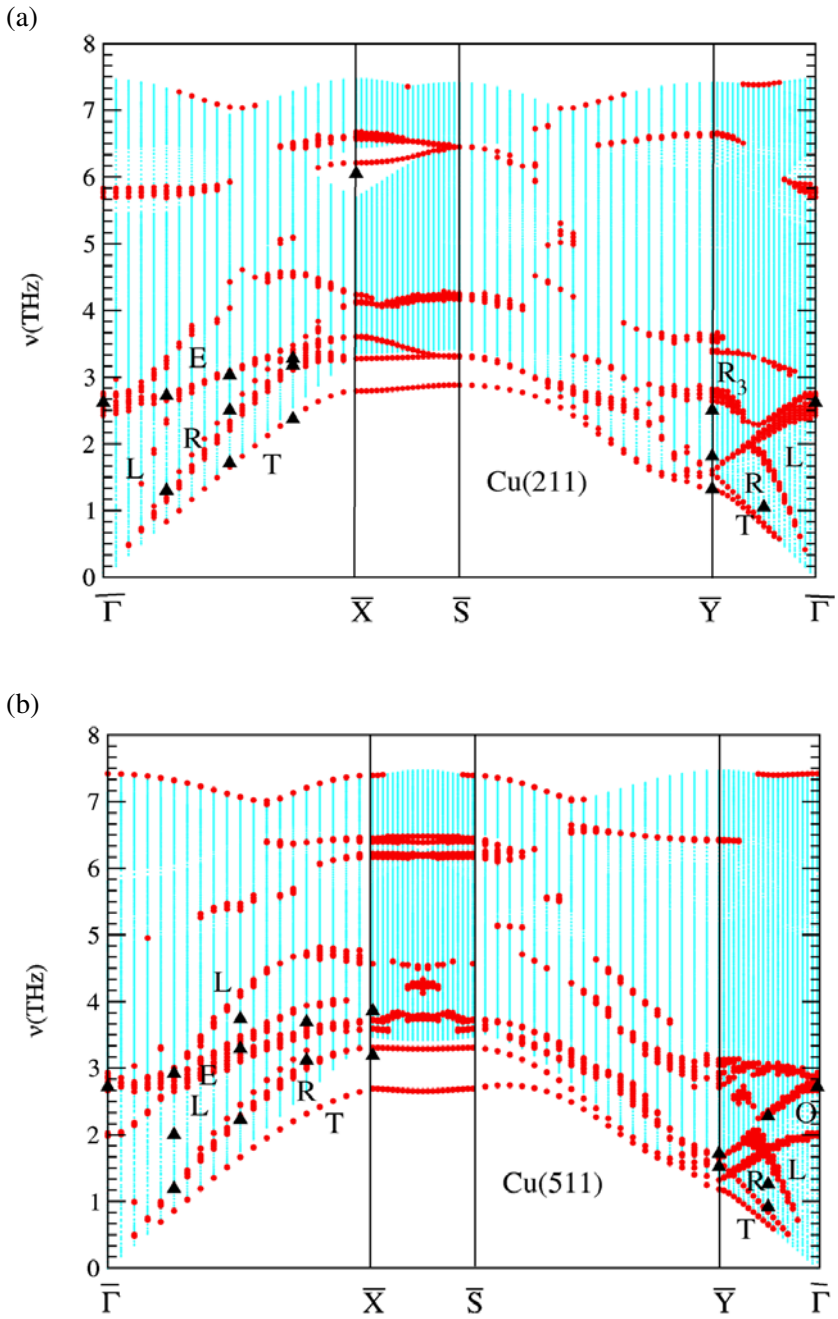

Figure 6. Frequency spectra of phonons for the (211) (a) and (511) (b) surfaces of Cu as a function of $\mathbf{k}_{\parallel}$ along a given path in the SBZ. Each segment is proportional to its length in the reciprocal space. Bulk states are represented by small dots. Localized and resonant states are denoted by heavy dots. The prominent surface features are denoted with the same notation as in [5] and the localization criterion is 6% on the first four layers. Experimental points are taken from [5] except for the highest frequency at $\bar{X}$ which corresponds to the EELS data of [6].

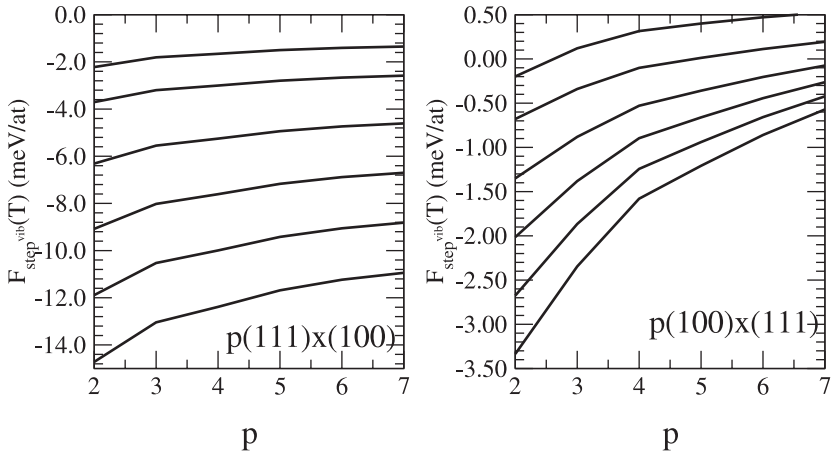

Figure 7. The contribution of vibrations to the step free energy for $p(100) \times (111)$ and $p(111) \times (100)$ vicinal surfaces as a function of p for the given temperatures.

4.4. Vibrational free energy of steps

The contribution of vibrations to the free energy of a system which has a total density of frequencies $n(\nu)$ is given by

$$F^{\mathrm{vib}}(T) = k_{\mathrm{B}}T \int_0^{\infty} \ln\left(2 \sinh \frac{h\nu}{2k_{\mathrm{B}}T}\right) n(\nu)\, \mathrm{d}\nu \tag{18}$$

where k_{B} is the Boltzmann constant. In the case of 2D periodicity, the integral over the frequency is carried out by summing over special $\mathbf{k}_{\parallel}$ points belonging to the irreducible SBZ. From the vibrational free energy of the vicinal surfaces, low index surfaces and bulk, the vibrational free energy of steps (per step atom) $F^{\mathrm{vib}}_{\mathrm{step}}(T)$ can be derived at any temperature using an equation similar to (11). We have calculated $F^{\mathrm{vib}}_{\mathrm{step}}(T)$ for $p(100) \times (111)$ and $p(111) \times (100)$ vicinal surfaces of increasing terrace widths, for temperatures ranging from 0 to 500 K. The step vibrational free energy of a given vicinal surface is of the order of a few millielectronvolts and decreases with temperature, reaching a linear regime for T larger than 100 K when the entropy contribution becomes the leading term (see [59]). More interestingly $F^{\mathrm{vib}}_{\mathrm{step}}(T)$ can be plotted for a given temperature as a function of the terrace width as shown in figure 7. It appears that $F^{\mathrm{vib}}_{\mathrm{step}}(T)$ decreases in absolute value when the terrace width increases, i.e., phonons produce attractive step–step interactions. Furthermore the absolute value of these attractive step–step interactions increases with temperature. The possibility of interactions between surface defects mediated by phonons has already been investigated by Cunningham *et al* [60] who have derived the phonon contribution to the free energy of interaction for an adatom pair on the (100) face of cubium using the Montroll–Potts model and also found an attractive interaction. Finally note that, even though the vibrational contribution to the step energy is of the order of a few millielectronvolts, and therefore quite negligible compared to the absolute value of the step energy, its variation with the vicinality can be of the same order of magnitude as the repulsive elastic one at least in the range of small terrace widths ($p < 10$). Figure 8 shows the variation of the step energy as a function of p including both the elastic and vibrational contributions at 300 K. The correction to the isolated step energy is small but phonons change the curvature of the step energy and, surprisingly, may even modify its sign. In particular for the $p(111) \times (100)$ surfaces the step energy exhibits a minimum at $p = 3$, i.e., the resulting step–step interactions are attractive.

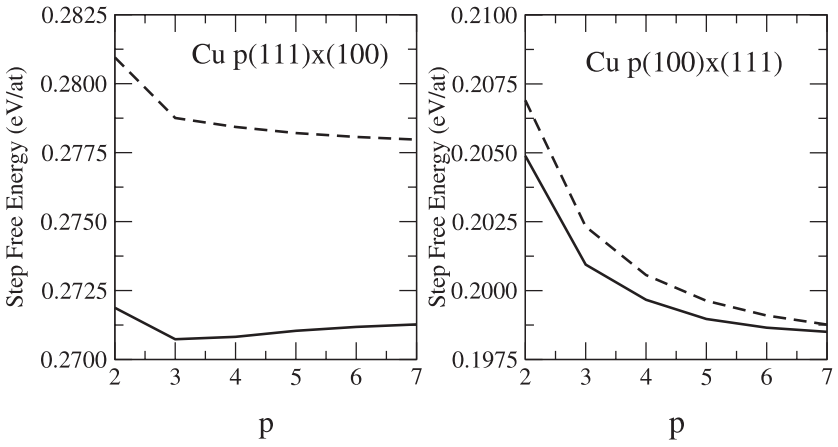

Figure 8. Variation of the step free energy at 300 K as a function of p without (dashed line) and with (full line) the vibrational contribution.

In addition, it must be kept in mind that electronic effects are far from being negligible, at least for small terrace widths (typically less than ten atomic rows) and usually give rise to oscillatory interactions as shown in the previous sections.

5. Stability of vicinal surfaces with respect to faceting

Vicinal surfaces are not always stable. Indeed, as seen in section 3, their surface energies γ are large and it might be energetically favourable for the solid to expose to vacuum low index facets with smaller surface energies per unit area, even if the total surface area is increased by the transformation. This phenomenon, called faceting, has been known for a long time [61]. The faceting condition implies calculation of the surface energy for any surface orientation, i.e., the knowledge of the γ-plot. Herring [24] was the first to propose a geometrical construction starting from the γ-plot and predicting the occurrence of faceting. Then this condition was recast in a much simpler way (see section 5.1). The simplest methods for calculating the surface energies as a function of the orientation range from the crudest empirical pair potentials to various semi-empirical ones (EAM, EMT, SMA, . . .), including an N body contribution, which have been set up in the last two decades. Recently, the stability of vicinal surfaces with respect to faceting was re-examined using the EMT potential [62]. It was shown that the total energy difference between the vicinal and faceted surface is very small and, surprisingly, it was found that all vicinal surfaces between the (100) and (111) planes were unstable, at least at 0 K, and that the observed stability at room temperature arises from the entropy contribution due to thermal vibrations. However semi-empirical potentials have a common drawback: they only depend on the inter-atomic distances and not on the angular arrangement of atoms. Although this latter effect is small in metals, it is not obvious that it can be neglected in view of the tiny energy difference involved in faceting. In [25, 26], we revisited this problem at 0 K and analysed the answers given by pair potentials, semi-empirical potentials and the TB calculations presented above (section 3). Finally our study of vibrational properties of vicinal surfaces (section 4) has enabled us to investigate the effect of finite temperatures.

In the following we first recall the faceting condition. Then we summarize our results concerning the possible faceting of the vicinal surfaces that are spanned when going from the (100) to the (111) plane. Other domains of orientations have been studied in [26].

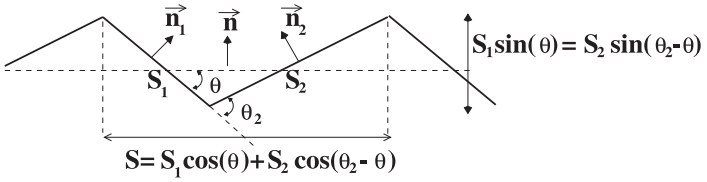

Figure 9. Faceting.

5.1. Faceting condition of an infinite surface

Let us consider two low index surfaces Σ_1 and Σ_2 with normals $\mathbf{n}_1$ and $\mathbf{n}_2$, respectively, which intersect along a given row of atoms and the set of vicinal surfaces with equidistant step edges which is spanned when Σ_1 is rotated around the common atomic row towards Σ_2. Let us take Σ_1 as the origin of angles and denote by θ_2 the angle $(\mathbf{n}_1, \mathbf{n}_2)$. During this rotation the surfaces vicinal to Σ_1 are first found and the number of atomic rows p_1 (including the inner edge) on one terrace decreases from ∞ to 2 (angle θ_c). The surface corresponding to θ_c can also be regarded as a vicinal of Σ_2 with $p_2 = 2$. Then for $\theta_c \leqslant \theta < \theta_2$ the surfaces vicinal to Σ_2 are scanned with increasing terrace widths ($p_2 \geqslant 2$). An area S of any of these high index surfaces will transform into facets of normal $\mathbf{n}_1$ (area S_1) and normal $\mathbf{n}_2$ (area S_2) while keeping its average orientation when (figure 9)

$$\gamma S > \gamma_1 S_1 + \gamma_2 S_2 \tag{19}$$

(γ, γ_1 and γ_2 being the surface energies per unit area of the high index, Σ_1 and Σ_2 surfaces, respectively) with the constraints

$$S = S_1 \cos\theta + S_2 \cos(\theta_2 - \theta), \tag{20}$$

$$S_1 \sin\theta = S_2 \sin(\theta_2 - \theta). \tag{21}$$

It is easily shown that the faceting condition can be written as

$$f(\eta) > (1 - \eta/\eta_2) f(0) + (\eta/\eta_2) f(\eta_2) \tag{22}$$

with $\eta = \tan\theta$ and $f(\eta) = \gamma(\theta)/\cos\theta$. This condition is equivalent to the Herring construction [26].

This inequality has a simple geometrical interpretation: the vicinal surface corresponding to η is unstable(stable) when the point $(\eta, f(\eta))$ is above (below) the straight line D joining the points $(0, f(0))$ and $(\eta_2, f(\eta_2))$ or, equivalently, the sign of the deviation $\Delta f(\eta)$ from this straight line determines the stability ($\Delta f(\eta) < 0$) or the instability ($\Delta f(\eta) > 0$) of the vicinal surface. By straightforward geometrical consideration, it is easily shown [26] that

$$\Delta f(\mathbf{n}) = [E_S(\mathbf{n}) - (p_1 - 1)E_S(\mathbf{n}_1) - (p_2 - 1)E_S(\mathbf{n}_2)]/A_0(\mathbf{n}) \tag{23}$$

where $A_0(\mathbf{n})$ is the projected area of the surface unit cell A of the vicinal surface of orientation $\mathbf{n}$ on Σ_1. This formula applies as well in the domain $0 \leqslant \theta \leqslant \theta_c$ with $p_2 = 2$ as when $\theta_c \leqslant \theta \leqslant \theta_2$ with $p_1 = 2$. $E_S(\mathbf{n})$ is the surface energy (per atom) of the surface normal to $\mathbf{n}$. It is interesting to note that the condition of instability of the surface corresponding to η_c (normal $\mathbf{n}_c$) is simply

$$E_S(\mathbf{n}_c) > E_S(\mathbf{n}_1) + E_S(\mathbf{n}_2). \tag{24}$$

We will see below that in many cases the sign of $\Delta f(\eta_c)$ determines the stability for the whole range $[0, \eta_2]$. It is clear that the sign of Δf is independent of the origin of angles, i.e., whether Σ_1 is referred to the angle θ_1, since it is given by the sign of the expression in the square brackets in equation (23) which will be denoted as $\Delta E(p_1, p_2)$ in the following.

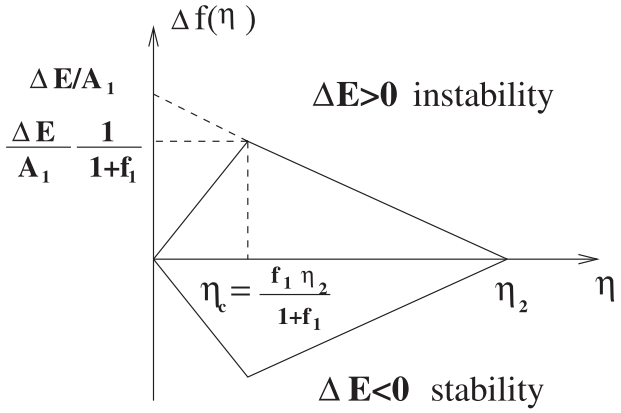

Figure 10. The behaviour of $\Delta f(\eta)$ when there are no interactions between steps. η_c corresponds to $p_1 = p_2 = 2$.

Let us denote by A_1 (A_2) the area of the unit cell of Σ_1 (Σ_2). It is straightforward to show that

$$\begin{aligned} \Delta f(\eta) &= \frac{\Delta E(p_1, 2)}{A_2 \sin\theta_2}\eta, \qquad 0 \leqslant \eta \leqslant \eta_c, \\ \Delta f(\eta) &= \frac{\Delta E(2, p_2)}{A_1}(1 - \eta/\eta_2), \qquad \eta_c \leqslant \eta \leqslant \eta_2. \end{aligned} \tag{25}$$

By using equation (11), $\Delta E(p_1, 2)$ can be transformed into:

$$\Delta E(p_1, 2) = E_{\text{step}}(\mathbf{n}_1, p_1) - E_S(\mathbf{n}_2) + f_1 E_S(\mathbf{n}_1) \tag{26}$$

(a similar equation can be written out for $\Delta E(2, p_2)$ by interchanging the indices 1 and 2 in the right-hand side of this equation). As seen in section 3, the step energy varies with p due to step–step interactions and, consequently, $\Delta E(p_1, 2)$ and $\Delta E(2, p_2)$ depend on η. When these interactions are neglected, these last two quantities are equal to their values at $p_1 = 2$ and $p_2 = 2$, or $\eta = \eta_c$. Then from (25) $\Delta f(\eta)$ has a triangular shape (figure 10). Any vicinal surface between Σ_1 and Σ_2 is unstable (stable) with respect to faceting when $\Delta E > 0$ ($\Delta E < 0$). In conclusion, any deviation of $\Delta f(\eta)$ from the triangular shape is a sign of the presence of interactions between steps. If for a given orientation η_0 such that $0 < \eta_0 < \eta_c$, $\Delta f(\eta_0)$ is above (below) the tangent to $\Delta f(\eta)$ at the origin, then the interactions between steps are repulsive (attractive). The same conclusion holds for $\eta_c < \eta_0 < \eta_2$ but the tangent has to be taken at $\eta = \eta_2$. In the domain that will be considered below and defined by $\mathbf{n}_1(100)$ and $\mathbf{n}_2(111)$, i.e., (100)–(111), η varies from 0 to $\eta_2 = \sqrt{2}$. When $0 < \eta \leqslant \eta_c$ ($\eta_c = \sqrt{2}/3$) the crystallographic planes $(2p - 1, 1, 1)$ are spanned and correspond to the $p(100) \times (111)$ surfaces and when $\eta_c \leqslant \eta < \eta_2$ ($\eta_2 = \sqrt{2}$) the crystallographic planes are $(p+1, p-1, p-1)$ and the corresponding vicinal surfaces are $p(111) \times (100)$ (see table 1). Note that for $\eta = \eta_c$ the Miller indices of the surface are (311).

5.2. Stability of vicinal surfaces at 0 K from semi-empirical potentials

Empirical potentials belonging to a very large class can be written as a sum of contributions E_i from each atom i (referred to the energy of a free atom, $E_i < 0$) depending on its environment

of neighbours j at the inter-atomic distance R_{ij}, i.e.

$$E = \sum_i E_i = \sum_i \left\{ \sum_{j \neq i} V(R_{ij}) + F\left(\sum_{j \neq i} g(R_{ij}) \right) \right\}. \tag{27}$$

E is the total energy of the system at 0 K neglecting the zero point vibrational energy. In the following we set $\rho_i = \sum_{j \neq i} g(R_{ij})$. The first term of equation (27) is thus pairwise while the second one (in which g is a positive function) has an N body character. The functions V and g are usually cut-off smoothly around a given radius R_c. This class of potentials includes pair potentials ($F(\rho_i) = 0$), potentials based on EMT [7, 8], the EAM [9] and the glue model [63] and potentials derived from the TB approximation in the second moment approach ($F(\rho_i) \propto \sqrt{\rho_i}$) [10–12] or in which $F(\rho_i) \propto \rho_i^\alpha$ ($\alpha \neq 1/2$). This law with $\alpha = 2/3$ has been proposed to account for the effect of higher order moments [64] and has been actually found for Cu when fitting the five parameters of the potential to experimental bulk quantities (see section 4 and [23]). Note that in potentials of the TB type, the N body part is strictly attractive while the pairwise part is strictly repulsive.

Some physical insight can be gained by fixing the inter-atomic distances to their bulk equilibrium values, i.e., ignoring atomic relaxation effects. With this assumption $\sum_{j \neq i} V(R_{ij})$ and $\sum_{j \neq i} g(R_{ij})$ are linear combinations of the number of neighbours Z_i^J of atom i in the Jth coordination sphere of radius R_J ($R_J < R_c$) and $E_i = E(Z_i^1, \ldots, Z_i^J, \ldots)$. It is usual to take R_1 as the reference distance and set $g(R_1) = 1$. From the discussion of section 5.1, we will first determine whether there is any interaction between steps. Obviously steps start to interact when the range of the potential is large enough. Then the two straight lines of figure 10 transform into as many segments (with discontinuities of slopes) as there are different step energies when p increases.

5.2.1. Pair potentials. These potentials are the simplest of the ones which have been used in the past. We will limit ourselves to the study of unrelaxed surfaces since it is well known that pair potentials most often lead to an outward relaxation instead of the inward one generally observed at metal surfaces. For any orientation of the surface it is easy to determine the coordination numbers $Z_i^1, Z_i^2, \ldots$ for the successive atomic layers i from which the numbers n_{step}^J are deduced. For the domain (100)–(111) it is found that there are no step interactions if $R_c < R_6$. Then $\Delta f(\eta)$ has the triangular shape of figure 10 and its sign on the whole domain $[0, \eta_2]$ is given by (see equation (24))

$$\Delta E = E_S(311) - E_S(100) - E_S(111) = -4(V_3 + V_5). \tag{28}$$

In conclusion, if $R_c < R_3$, $\Delta E = 0$, so the energy of any vicinal surface is equal to the energy of the faceted (100)/(111) surface. If $R_c < R_6$, the surface is unstable if $V_3 + V_5 < 0$ and stable otherwise.

5.2.2. N body semi-empirical potentials. We now examine the case of semi-empirical potentials including an N body contribution and begin by neglecting atomic relaxation in order to derive general trends for potentials of type (27). Then we will present a study of the stability of Cu vicinal surfaces in the (100)–(111) domain using the semi-empirical potential set up in section 4.1.

When the inter-atomic distances are fixed to their bulk equilibrium values, the energy of an atom i, $E_i(Z_i^1, \ldots, Z_i^J, \ldots)$, is no longer a linear function of Z_i^J. However as will be seen below, the mathematical properties of the function F have interesting physical consequences.

It can be shown easily that the step energies of $p(100) \times (111)$ and $p(111) \times (100)$ are independent of p as long as $R_c < R_3$ and are given by

$$E_{\text{step}}^{p(100)\times(111)} = E(7,3) + E(10,5) - 3E(8,5)/2 - E(12,5)/2 \tag{29}$$

and:

$$E_{\text{step}}^{p(111)\times(100)} = E(7,3) - 5E(9,3)/3 + E(10,5) + E(12,5) - 4E(12,6)/3. \tag{30}$$

Consequently for any semi-empirical potential of the form (27) including first and second nearest neighbours only, $\Delta f(\eta)$ has a triangular shape when atomic relaxation is neglected and its sign is given by

$$\Delta E = E_S(311) - E_S(100) - E_S(111) \tag{31}$$

or

$$\Delta E = [E(7,3) + E(10,5)] - [E(8,5) + E(9,3)]. \tag{32}$$

Thus, in this approximation, ΔE arises from the difference of the sum of energies of, on the one hand, atoms belonging to the outer ($Z_i^1 = 7$, $Z_i^2 = 3$) and inner ($Z_i^1 = 10$, $Z_i^2 = 5$) step edges and, on the other hand, (100) ($Z_i^1 = 8$, $Z_i^2 = 5$) and (111) ($Z_i^1 = 9$, $Z_i^2 = 3$) surface atoms.

As shown in section 5.2.1 the pair potential, when limited to second nearest neighbours, does not contribute to ΔE. Noting that, since we have chosen $g(R_1) = 1$, $\rho_i = Z_i^1 + Z_i^2 g_2$ with $g_2 = g(R_2)$, we get

$$\Delta E = [F(7 + 3g_2) - F(9 + 3g_2)] - [F(8 + 5g_2) - F(10 + 5g_2)]. \tag{33}$$

For all the existing potentials of the form (27) $F''(\rho) = \mathrm{d}^2F/\mathrm{d}\rho^2$ is positive. As a consequence $F(\rho - 2) - F(\rho)$ is a decreasing function of ρ; therefore ΔE (and thus $\Delta f(\eta)$) is always positive in the whole domain. This common property of this class of potentials has a clear physical origin: the energy E_i of an atom i should decrease more and more slowly when its coordination increases towards the bulk coordination [59, 65]. This clearly implies that $F''(\rho)$ must be positive. We have then proved that for *any* semi-empirical potential of the general form (27) on a rigid lattice at 0 K and with a cut-off radius $R_c < R_3$, *any* metal vicinal surface between (100) and (111) is *unstable* with respect to faceting.

So far we have demonstrated general results on the stability of vicinal surfaces neglecting atomic relaxation. These results were obtained under the assumption that the range of the potential is restricted to the first two shells of neighbours. As shown in [26] it is not possible to derive a general behaviour when the range of interactions is extended to further neighbours. In order to investigate the effect of atomic relaxation and of the range of interactions, it is necessary to have an explicit expression for the potential. We will now present the results obtained for Cu with the semi-empirical potential (P_2) of section 4 whose range is limited to first and second neighbours. In addition we have also considered the potential (P_4) of the same type ($\alpha = 2/3$) but with a cut-off radius between fourth and fifth neighbours with parameters obtained from a least mean squares fit of the cohesive energy, the three elastic constants and the bulk equilibrium distance. In all cases the atomic structure of each vicinal surface has been fully relaxed using a conjugate gradient algorithm.

The results are given in figure 11 for the (100)–(111) domain using both potentials and relaxed as well as unrelaxed surfaces. As predicted from our previous analysis in the unrelaxed case $\Delta f(\eta)$ has a triangular shape and is positive if the range of the potential is restricted to second neighbours (P_2). However as expected, due to the effect of further neighbours $\Delta f(\eta)$ deviates from a triangular shape with potential P_4 and, more surprisingly, it changes sign. Thus all vicinal surfaces between (100) and (111) become stable.

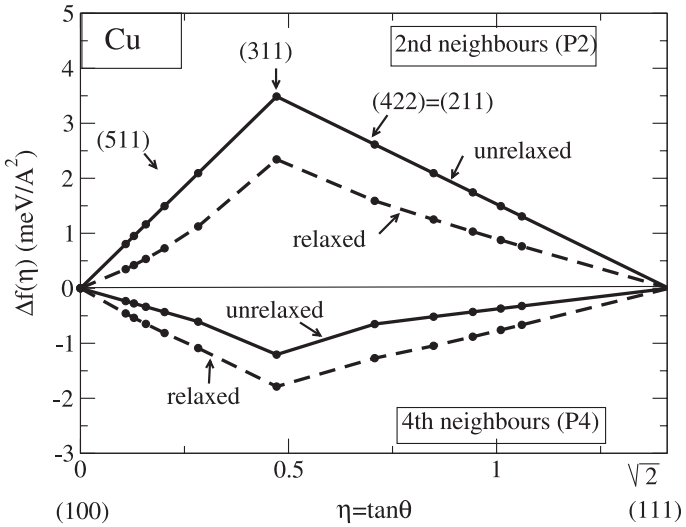

Figure 11. $\Delta f(\eta)$ for Cu derived from the semi-empirical potentials P_2 and P_4 given in the text corresponding to two cut-off radii with and without relaxation for the (100)–(111) domain.

Finally, atomic relaxation always acts in favour of the stabilization of vicinal surfaces since the atomic displacements are larger on a vicinal surface than on a flat one (see section 4). Nevertheless this effect is not large enough to modify the stability or instability of the vicinal surfaces. Furthermore, as clearly seen when using potential P_2 in the relaxed case, $\Delta f(\eta)$ no longer has a triangular shape and is entirely located above the triangle built from its tangent at both ends due to the repulsive elastic step–step interactions (see section 4).

Let us discuss and summarize our results. From our analytical study and figure 11 it appears that the range of the potential plays an important role but it is difficult to draw general conclusions. In all cases considered here the effect of further neighbours is to act in favour of the stabilization of vicinal surfaces; however including them will not automatically make vicinal surfaces stable—this crucially depends on their relative importance and, therefore, on the dependence of the functions $V(r)$ and $g(r)$ on distance in (27). The stability also depends on the relative importance of V with respect to $F(\rho)$ since, when further neighbours are included, both terms are present in the energy balance. Moreover, in EAM and EMT potentials the N body and pair parts are not necessarily purely attractive or purely repulsive; therefore even the sign of these terms is not known. Let us finally compare our results with those of Frenken and Stoltze [62]. These authors have calculated $\Delta f(\eta)$ for the fully relaxed (100) and (111) vicinal surfaces of Ag (and other metals) using an EMT potential with $R_3 < R_c < R_4$ but in which the contribution of third neighbours is nearly negligible. This explains the strong similarity between our results on relaxed Cu (figure 11) with potential P_2 and those of Frenken and Stoltze for Ag.

In conclusion, the instability of vicinal surfaces at 0 K claimed by these authors is an *unavoidable* consequence of the type of potential used when interactions are limited to first and second neighbours.

5.3. Stability of vicinal surfaces at 0 K from tight binding calculations

It is interesting to deduce the function $\Delta f(\eta)$ from the results presented in section 3. Indeed, the TB calculations are certainly more realistic than those based on semi-empirical potentials since

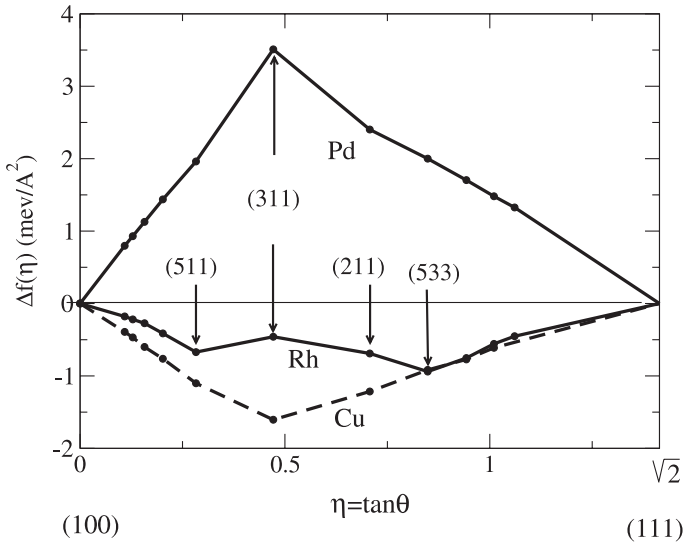

Figure 12. $\Delta f(\eta)$ for Rh, Pd and Cu from TB calculations for the (100)–(111) domain.

they account for the influence of the angular arrangement of neighbours and include electronic step–step interactions (often oscillatory). We have seen in section 3 that these interactions are small. However they may play a role in the very delicate energy balance which governs the stability of vicinal surfaces.

The functions $\Delta f(\eta)$ for Rh, Pd and Cu in the (100)–(111) domain are plotted in figure 12 and show very different behaviours depending on the chemical element. For Cu all vicinal surfaces in the domain are stable at 0 K while for Pd they are unstable. Rh behaves quite differently: even though all vicinal surfaces are stable with respect to faceting into (100) and (111) facets, the vicinal surfaces of orientation such that $\sqrt{2}/5 < \eta < 3\sqrt{2}/5$ are unstable relative to faceting into (511) and (533) orientations which correspond to the two local minima in $\Delta f(\eta)$. This peculiar behaviour is clearly related to the electronic step–step interactions which are repulsive for the (311) and (211) surfaces and attractive for (511) and (533) surfaces (see figure 2).

5.4. Finite temperature effects

So far all calculations were carried out at 0 K. Therefore it is important to know whether the effect of a finite temperature may be large enough to reverse the stability of vicinal surfaces with respect to faceting. The variation of $f(\eta)$ with temperature arises from two contributions: the vibrational effects that have been studied in section 4 and the meandering of steps, which is regulated by the kink formation energy, giving rise to entropy contributions. Let us first discuss the order of magnitude of the latter. In the limit of infinite terraces steps fluctuate independently of each other but when the terrace width decreases the entropy gain due to the meandering is limited by the non-crossing condition which gives rise to a repulsive step–step interaction. Actually, both effects are driven by a parameter $\zeta = \exp(-\epsilon_{\text{kink}}/k_{\text{B}}T)$ where ϵ_{kink} is the kink formation energy. As can be seen from table 4 this parameter is quite small, at least up to room temperature and, as a consequence, these two contributions are negligible compared with the value of $\Delta f(\eta)$ at 0 K and they are also small compared with the contribution $\Delta f_{\text{vib}}(\eta)$ due to vibrations [26].

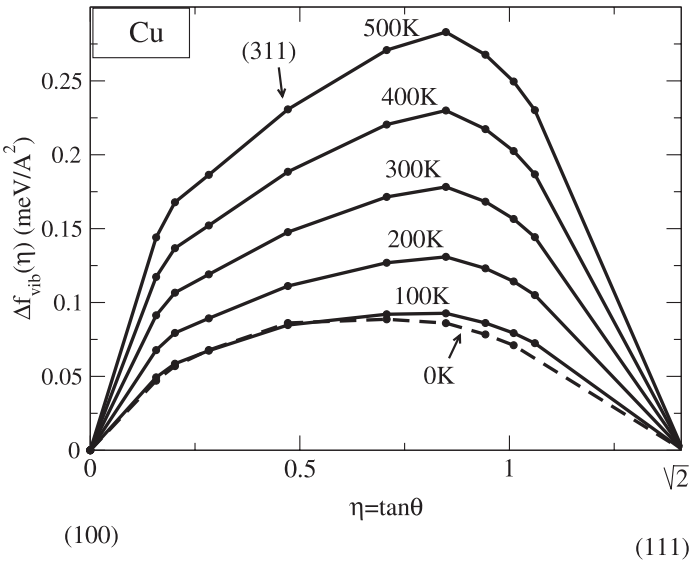

Figure 13. $\Delta f_{\mathrm{vib}}(\eta)$ in the (100)–(111) domain from potential P_2 as a function of temperature.

From the study of vibrations presented in section 4, we can easily derive $\Delta f_{\mathrm{vib}}(\eta)$ as a function of temperature in the (100)–(111) domain. The corresponding curves for copper are drawn in figure 13. It can be seen that Δf_{vib} is positive but its order of magnitude is not large enough to destabilize the vicinal surfaces of Cu in this domain. These results are in contradiction with those of Frenken and Stoltze [62]. Actually these authors evaluated the vibrational entropy contribution using a simplified Einstein model and neglected the vibrational internal energy which is justified at room temperature, but not at low temperature. More importantly they only included the perturbation between the outer edge and a (111) surface atom and not the term coming from the perturbation between the inner edge and the (100) surface atom (see equation (32)). These two terms are of opposite sign and are expected to be of the same order of magnitude. Consequently not only is the estimate of Δf_{vib} in [62] too large but even the sign is wrong.

In conclusion, the contribution of the vibrations Δf_{vib} to Δf is quite small. Thus its calculation needs a precise knowledge of the phonon spectra including both vibrational internal energy and entropy, at least if the temperature varies from 0 K to $\simeq$300 K.

6. Conclusions

In conclusion, with the spd TB method it is possible to carry out realistic calculations on the energetics of vicinal surfaces: surface, step and kink energies. Indeed, the formation energies of isolated steps, obtained with this method, on Rh, Pd and Cu surfaces for various geometries are in good agreement with existing experimental data. In particular, our results predict that an adisland of Cu on Cu(100) should be a square with broken corners at 0 K. Moreover the correct relative stability of the two types of step (A and B) on the vicinal surfaces of Cu(111) is obtained. Kink energies have also been calculated and compare nicely with experimental data.

Following the approach of Vitos *et al* [34] and from the knowledge of the surface energies of the three low index surfaces calculated from the spd TB Hamiltonian, effective pair interactions

can be deduced giving step and kink energies in good agreement with those derived from the diagonalization of the same Hamiltonian for vicinal surfaces. However in this approach step–step interactions are disregarded. In contrast, our study, based on the calculation of step energies on vicinal surfaces as a function of the terrace width, has enabled us to derive electronic step–step interactions for narrow and moderately wide terraces ($d \leqslant 20$ Å). These interactions are rapidly decaying and they may be attractive or repulsive depending on the terrace width. Moreover, in this range of widths, their order of magnitude is comparable to that of other interactions.

A semi-empirical potential for copper, including an N body contribution, has been built. It accounts for the multilayer relaxation of vicinal surfaces and describes accurately their localized vibration modes observed in IHAS and EELS. The contribution of vibrations to the free energy of steps has also been calculated as a function of the distance between steps and it was found that the step–step interactions mediated by phonons are attractive for Cu vicinal surfaces in the (100)–(111) domain.

The stability of vicinal surfaces with respect to faceting has also been investigated. The conclusions derived from semi-empirical potentials have been analysed and criticized. In contrast to the results obtained from these potentials which predict that vicinal surfaces of metals are unstable at 0 K, the TB electronic structure calculations lead to a variety of behaviours: a vicinal surface in the (100)–(111) domain may be stable (Cu) or unstable (Pd) relative to faceting into (100) and (111) facets or may even undergo a faceting towards other vicinal surfaces (Rh). Finally, temperature effects have been found to be negligible for Cu, at least up to room temperature.

References

[1] Giesen M 2001 *Prog. Surf. Sci.* **68** 1 and references therein
[2] Pai W W, Ozcomert J S, Bartelt N C, Einstein T L and Reutt-Robey J E 1994 *Surf. Sci.* **307–309** 747
[3] Villain J, Grempel D R and Lapujoulade J 1985 *J. Phys. F: Met. Phys.* **15** 809
[4] Barbier L, Masson L, Cousty J and Salanon B 1996 *Surf. Sci.* **345** 197
[5] Witte G, Braun J, Lock A and Toennies J P 1995 *Phys. Rev.* B **52** 2165
[6] Kara A, Staikov P, Rahman T S, Radnik J, Biagi R and Ernst H J 2000 *Phys. Rev.* B **61** 5714
[7] Jacobsen K W, Norskov J K and Puska M J 1987 *Phys. Rev.* B **35** 7423
Jacobsen K W, Stoltze P and Norskov J K 1996 *Surf. Sci.* **366** 394
[8] Stoltze P 1994 *J. Phys.: Condens. Matter* **6** 9445
[9] Daw M S and Baskes M I 1984 *Phys. Rev.* B **29** 6443
[10] Ducastelle F 1970 *J. Physique* **31** 1055
[11] Sutton A P and Chen J 1984 *Phil. Mag. Lett.* **61** 139
[12] Finnis M W and Sinclair J E 1984 *Phil. Mag.* A **50** 45
[13] Nelson J S and Feibelman P J 1992 *Phys. Rev. Lett.* **68** 2188
[14] Stumpf R and Scheffler M 1996 *Phys. Rev.* B **53** 958
[15] Feibelman P J 1999 *Phys. Rev.* B **60** 11118
[16] Spisák D 2001 *Surf. Sci.* **489** 151
[17] Feibelman P J 2000 *Surf. Sci.* **463** L661
[18] Raouafi F, Barreteau C, Desjonquères M C and Spanjaard D 2002 *Surf. Sci.* **505** 183
[19] Chen Y, Tong S Y, Kim J S, Kesmodel L S, Rodach T, Bohnen K P and Ho K M 1991 *Phys. Rev.* B **44** 11394
[20] Wei C Y, Lewis S P, Mele E J and Rappe A M 1998 *Phys. Rev.* B **57** 10062
[21] Kara A, Durukanoglu S and Rahman T S 1996 *Phys. Rev.* B **53** 15489
[22] Sklyadneva I Yu, Rusina G G and Chulkov E V 1998 *Surf. Sci.* **416** 17
[23] Barreteau C, Raouafi F, Desjonquères M C and Spanjaard D 2002 *Surf. Sci.* **519** 15
[24] Herring C 1951 *Phys. Rev.* **82** 87
[25] Desjonquères M C, Spanjaard D, Barreteau C and Raouafi F 2002 *Phys. Rev. Lett.* **88** 056104
[26] Raouafi F, Barreteau C, Spanjaard D and Desjonquères M C 2002 *Phys. Rev.* B **66** 045410
[27] Lang B, Joyner R W and Somorjai G A 1972 *Surf. Sci.* **30** 440

[28] Mehl M J and Papaconstantopoulos D A 1996 *Phys. Rev.* B **54** 4519
[29] Barreteau C, Spanjaard D and Desjonquères M C 1998 *Phys. Rev.* B **58** 9721
[30] Slater J C and Koster G F 1954 *Phys. Rev.* **94** 1498
[31] Barreteau C, Guirado-López R, Spanjaard D, Desjonquères M C and Oleś A M 2000 *Phys. Rev.* B **61** 7781
[32] The parameters of [28] are available on the web-site http://cst-www.nrl.navy.mil/bind/
[33] Cunningham S L 1974 *Phys. Rev.* B **10** 4988
[34] Vitos L, Skriver H L and Kollar J 1999 *Surf. Sci.* **425** 212
[35] Weinert M and Davenport J W 1992 *Phys. Rev.* B **45** 13709
[36] Methfessel M, Henning D and Scheffler M 1992 *Phys. Rev.* B **46** 4816
[37] Eichler A, Hafner J, Furthmüller J and Kresse G 1996 *Surf. Sci.* **346** 300
[38] Galanakis I, Bihlmayer G, Bellini V, Papanikolaou N, Zeller R, Blügel S and Dederichs P H 2002 *Europhys. Lett.* **58** 751
Galanakis I, Papanikolaou N and Dederichs P H 2002 *Surf. Sci.* **511** 1
[39] Schlösser D C, Verheij L K, Rosenfeld G and Comsa G 1999 *Phys. Rev. Lett.* **82** 3843
[40] Icking-Konert G S, Giesen M and Ibach H 1999 *Phys. Rev. Lett.* **83** 3880
[41] Marchenko V I and Parshin Y A 1981 *Sov. Phys.—JETP* **52** 129
[42] Tian Z T and Rahman T S 1993 *Phys. Rev.* B **47** 9751
[43] Wolf D and Jaszczaki J 1992 *Surf. Sci.* **277** 301
[44] Najafabadi R and Srolovitz D J 1994 *Surf. Sci.* **317** 221
[45] Hecquet P and Salanon B 1996 *Surf. Sci.* **366** 415
[46] Jayaprakash C, Rottman C and Saam W F 1984 *Phys. Rev.* B **30** 6549
[47] Hasegawa Y and Avouris P H 1993 *Phys. Rev. Lett.* **71** 1071
[48] Einstein T L and Schrieffer J R 1973 *Phys. Rev.* B **7** 3629
[49] Yaniv A 1981 *Phys. Rev.* B **24** 7093
[50] Frohn J, Giesen M, Poensgen M, Wolf J F and Ibach H 1991 *Phys. Rev. Lett.* **67** 3543
[51] Redfield A C and Zangwill A 1992 *Phys. Rev.* B **46** 4289
[52] Xu W, Adams J B and Einstein T L 1996 *Phys. Rev.* B **54** 2910
[53] Papadia S, Desjonquères M C and Spanjaard D 1996 *Phys. Rev.* B **53** 4083
[54] Liu C L and Adams J B 1993 *Surf. Sci.* **294** 211
[55] Nicklow R M, Gilat G, Smith H G, Raubenheimer L J and Wilkinson M K 1967 *Phys. Rev.* **64** 922
[56] Prévot G, Cohen C, Schmaus D, Hecquet P and Salanon B 2002 *Surf. Sci.* **506** 272
[57] Shilkrot L E and Srolovitz D J 1996 *Phys. Rev.* B **53** 11120
[58] Armand G and Masri P 1983 *Surf. Sci.* **130** 89
[59] Desjonquères M C and Spanjaard D 1996 *Concepts in Surface Physics* (Heidelberg: Springer)
[60] Cunningham S L, Dobrzynski L and Maradudin A A 1973 *Phys. Rev.* B **7** 4643
[61] Rosenhain W 1902 *Proc. R. Soc.* A **70** 252
[62] Frenken J W M and Stoltze P 1999 *Phys. Rev. Lett.* **82** 3500
[63] Ercolessi F, Parrinello M and Tosatti E 1988 *Phil. Mag.* A **58** 213
[64] Guevara J, Llois A M and Weissmann M 1995 *Phys. Rev.* B **52** 11509
[65] Robertson I J, Payne M C and Heine V 1991 *Europhys. Lett.* **15** 301